Contribution from the Departments of Inorganic Chemistry and Magnetism, Indian Association for the Cultivation of Science, Calcutta 700 032, India

Structure of Blue-Violet OsX_2L_2 and Its Reactions with Bidentate Ligands (D^{z-}): Spectra and Electrochemistry of $OsDL_2^{(2-z)+}$ [X = Cl, Br; L = 2-(*m*-Tolylazo)pyridine; *z* = 0–2]

BARINDRA KUMAR GHOSH,[1a] ANURADHA MUKHOPADHYAY,[1b] SREEBRATA GOSWAMI,[1a] SIDDHARTHA RAY,[1b] and ANIMESH CHAKRAVORTY*[1a]

Received March 12, 1984

The title complex (X = Cl), $OsCl_2(C_{12}H_{11}N_3)_2$, has been studied by X-ray crystallography. The compound forms monoclinic crystals in the space group $P2_1/c$ with $Z = 4$ and unit cell dimensions $a = 8.035$ (2) Å, $b = 24.176$ (4) Å, $c = 13.416$ (5) Å, $\beta = 114.34$ (3)°, and $V = 2374$ (3) Å^3. The structure was refined to $R_1 = 0.026$ and $R_2 = 0.037$. The Cl,Cl, N(imine),N(imine), and N(azo),N(azo) pairs, respectively, span cis, trans, and cis positions around octahedral osmium(II). The Os–N distances follow the order N(azo) < N(imine). The N–N bond length increases by ~0.06 Å on complexation. Presence of strong Os–N(azo) π bonding is implicated. The bromo complex (X = Br) reacts with bidentate N,N (azoimine and α-diimine species), O,O (oxalate and β-diketonate ions), and O,N (glycinate ion) ligands, affording complexes of the type $OsDL_2^{(2-z)+}$, which when charged are isolated as perchlorate salts. In the case of N,N ligands, the reaction is very slow and stereochemical rearrangement occurs (^{1}H NMR data). All complexes display singlet and triplet MLCT transitions in the visible region and undergo electrochemical metal oxidation and ligand reduction. The O,O complexes show osmium(IV)–osmium(III) and osmium(III)–osmium(II) couples in the range 1–2 V vs. SCE. For the N,N species only the latter couple is observable. Ligand reduction occurs in successive steps in the potential range +0.2 to −2.5 V. The N,N ligands provide one redox orbital for each azoimine/α-diimine group. Complete or nearly complete electron-transfer series have been identified.

Introduction

This work stems from our interest in the platinum metal azoimines symbolized in the chelate ring **1**. The azoimine

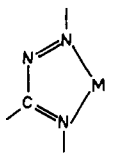

1

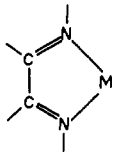

2

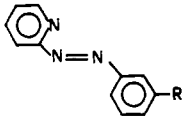

3

function is isoelectronic with the α-diimine function (as in **2**) present in, e.g., 2,2′-bipyridine (bpy). The platinum metal chemistry of two groups of azoimine ligands has been explored recently—the arylazo oximes[2-5] and 2-(arylazo)pyridines.[5-12]

Table I. Distances (Å) and Angles (deg) in the Coordination Octahedron of *trans,cis*-$OsCl_2(tap)_2$ (Estimated Standard Deviations in Parentheses)

	Distances		
Os-Cl(1)	2.399 (2)	Os-N(2)	2.055 (6)
Os-Cl(2)	2.393 (2)	Os-N(3)	1.972 (6)
Os-N(1)	2.075 (6)	Os-N(4)	1.975 (6)
	Angles		
Cl(1)-Os-Cl(2)	89.3 (1)	Cl(2)-Os-N(3)	89.3 (2)
Cl(1)-Os-N(1)	95.0 (2)	N(1)-Os-N(3)	75.9 (3)
Cl(1)-Os-N(2)	87.3 (2)	N(1)-Os-N(4)	101.4 (3)
Cl(1)-Os-N(4)	91.6 (2)	N(2)-Os-N(3)	101.9 (3)
Cl(2)-Os-N(1)	87.4 (2)	N(2)-Os-N(4)	76.3 (3)
Cl(2)-Os-N(2)	94.9 (2)	N(3)-Os-N(4)	91.2 (3)

The ruthenium complexes of these ligands are now known in some detail.[2,3,6-12] Considering the particular case of 2-(arylazo)pyridines (**3**), pseudooctahedral dihalo species of type MX_2L_2 can in principle occur in five geometrically isomeric forms.[6,11] Two and three of these respectively have the MX_2 group in trans and cis geometries. The geometries of the N(pyridine),N(pyridine) and N(azo),N(azo) pairs in the three *cis*-MX_2 complexes are trans,cis (tc, **4**), cis,trans (ct, **5**), and

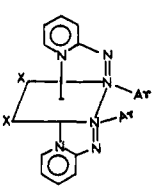

trans-cis (tc)
4

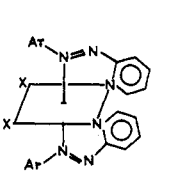

cis-trans (ct)
5

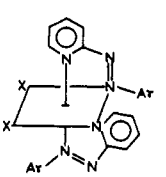

cis-cis (cc)
6

cis,cis (cc, **6**). The idealized symmetries of these are respectively C_2, C_2, and C_1. Of the five possible isomers, RuX_2L_2 actually affords only three: of these, one is most probably all trans.[6,11] The structures of the remaining two isomers (X = Cl, L = pap) are accurately known[14] from X-ray work to be

(1) (a) Department of Inorganic Chemistry. (b) Department of Magnetism.
(2) Chakravarty, A. R.; Chakravorty, A. *Inorg. Chem.* **1981**, *20*, 3138. Chakravarty, A. R.; Chakravorty, A. *J. Chem. Soc., Dalton Trans.* **1983**, 961.
(3) Chakravarty, A. R.; Chakravorty, A.; Cotton, F. A.; Falvello, L. R.; Ghosh, B. K.; Lisbona, M. T. *Inorg. Chem.* **1983**, *22*, 1892.
(4) Kalia, K. C.; Chakravorty, A. *Inorg. Chem.* **1969**, *8*, 2586. Mascharak, P. K.; Chakravorty, A. *J. Chem. Soc., Dalton Trans.* **1980**, 1698. Bandyopadhyay, P.; Mascharak, P. K.; Chakravorty, A. *Inorg. Chim. Acta Lett.* **1980**, *45*, L219. Bandyopadhyay, P.; Mascharak, P. K.; Chakravorty, A. *J. Chem. Soc., Dalton Trans.* **1981**, 623. *Ibid.* **1982**, 675. Bandyopadhyay, D.; Bandyopadhyay, P.; Chakravorty, A.; Cotton, F. A.; Falvello, L. R. *Inorg. Chem.* **1983**, *22*, 1315. Bandyopadhyay, D.; Bandyopadhyay, P.; Chakravorty, A.; Cotton, F. A.; Falvello, L. R. *Inorg. Chem.* **1984**, *23*, 1785.
(5) Bandyopadhyay, P.; Bandyopadhyay, D.; Chakravorty, A.; Cotton, F. A.; Falvello, L. R.; Han, S. *J. Am. Chem. Soc.* **1983**, *105*, 6327.
(6) Goswami, S.; Chakravarty, A. R.; Chakravorty, A. *Inorg. Chem.* **1981**, *20*, 2246.
(7) Goswami, S.; Chakravarty, A. R.; Chakravorty, A. *Inorg. Chem.* **1982**, *21*, 2737.
(8) Goswami, S.; Chakravarty, A. R.; Chakravorty, A. *J. Chem. Soc., Chem. Commun.* **1982**, 1288.
(9) Goswami, S.; Chakravarty, A. R.; Chakravorty, A. *Inorg. Chem.* **1983**, *22*, 602.
(10) Goswami, S.; Mukherjee, R. N.; Chakravorty, A. *Inorg. Chem.* **1983**, *22*, 2825.
(11) Krause, R. A.; Krause, K. *Inorg. Chem.* **1980**, *19*, 2600.
(12) Krause, R. A.; Krause, K. *Inorg. Chem.* **1982**, *21*, 1714.
(13) Ghosh, B. K.; Goswami, S.; Chakravorty, A. *Inorg. Chem.* **1983**, *22*, 3358.
(14) Seal, A.; Ray, S. *Acta Crystallogr., Sect. C: Cryst. Struct. Commun.*, in press.

0020-1669/84/1323-4633$01.50/0

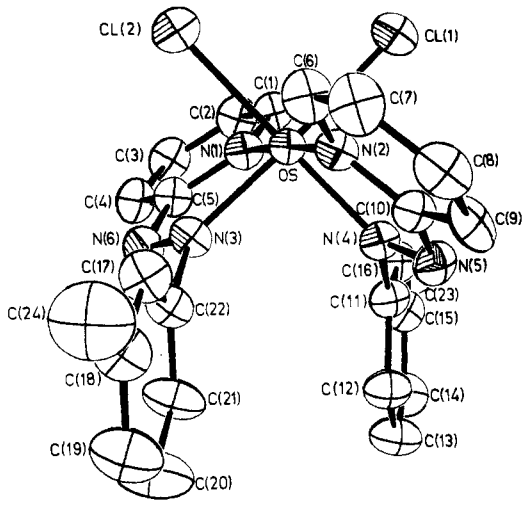

Figure 1. Atom-labeling scheme and 50% probability ellipsoids of *trans,cis*-$OsCl_2(tap)_2$.

tc (**4**) and cc (**6**). The dihalo complexes are precursors for the synthesis of many other complexes of L afforded by direct reaction or through the intermediacy of the diaquo derivative.[7,9,10,12] Ligand L is recognized[10,12,15] as a good π acceptor.

Progress in ruthenium azoimine chemistry has encouraged us to explore the corresponding osmium chemistry. This chemistry was completely unknown until our recent noting[13] of the two isomers of OsX_2L_2—one blue-violet and the other red-violet in solution. These were respectively assigned the tc (**4**) and cc (**6**) geometries on the basis of IR and ^1H NMR data. A definitive assignment based on three-dimensional X-ray structure determination of the blue-violet isomer of $OsCl_2(tap)_2$ is now reported. This rather than the pap complex was examined since the stereochemical assignment[13] based on ^1H NMR data (Me signal) applies directly to this complex. This work has helped to ascertain the relative π-donor abilities of ruthenium(II) and osmium(II) and to pinpoint a region in the case of **1** where the major M–L π interaction is localized. The use of blue-violet OsX_2L_2 for preparing new osmium tris complexes via reaction 1 in which D is a neutral or anionic (z = 0–2) bidentate oxygen and/or nitrogen donor ligand is examined. The spectral and redox properties of the new species are examined.

$$OsX_2L_2 + D^{z-} \rightarrow OsDL_2^{(2-z)+} + 2X^- \qquad (1)$$

Results and Discussion

A. Structure of Blue-Violet $OsCl_2(tap)_2$: π Bonding. Discrete molecules constitute the crystal. A view of the molecule is given in Figure 1. The coordination sphere around osmium is approximately octahedral, and the atomic arrangement indeed corresponds to the tc configuration. The halves of the molecule are very similar but not identical. The structure indeed approaches very closely the idealized C_2 symmetry. Selected bond angle data are in Table I.

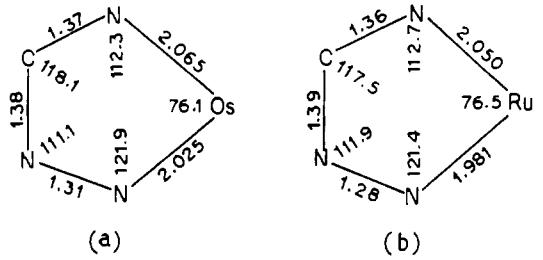

Figure 2. Average dimensions of chelate rings in esd: (a) of Os–N distances 0.006 Å, of C–N and N–N distances 0.01 Å, maximum of an angle 0.7°; (b) of Ru–N distances 0.005 Å, of C–N and N–N distances 0.01 Å, maximum of an angle 0.6°.

The two atomic groups Os, Cl(1), N(1), N(2), N(3) and Os, Cl(2), N(1), N(2), N(4) separately constitute two excellent and nearly orthogonal (dihedral angle ~88°) planes, with no atom deviating by >0.04 Å in either case. On the other hand, the planarity of the group Os, Cl(1), Cl(2), N(3), N(4) is not as good due to relatively large deviations (~0.3 Å) of N(3) and N(4) from the best plane in opposite directions. These deviations, which no doubt originate from the acute (~76°) chelate bite angle, also help in accommodating the two adjacent *m*-tolyl rings. It is remarkable that most of the distorsions away from octahedral positions arising out of the small bite angle are associated with the azo nitrogens whereas the pyridine nitrogens occupy nearly ideal axial positions [N(1)–Os–N(2) = 176.8 (2)°]. Each chelate ring is a good plane, with no atom deviating by more than 0.08 Å. The dihedral angle between the chelate ring and the corresponding *m*-tolyl ring is 54° in one case and 51° in the other.

The N–N distance in uncoordinated L is not available. However, it is very likely to be ~1.25 Å since the distances in PhN=NPh,[20] MeN=NMe,[21] and MeC(=NOH)N=NPh[22] are, respectively, 1.253 (3), 1.254 (3), and 1.256 (2) Å. Coordination can lead to a decrease in the N–N bond order due to both σ-donor and π-acceptor characters of the ligand—the latter character having a more pronounced[23] effect. The relatively long N–N distance in the osmium complex is thus indicative of the existence of considerable Os–L π bonding with major involvement of the azo group.

The difference in the status of the azo and imine functions with respect to π bonding is revealed even more clearly on comparing the mean light-atom bond parameters in the chelate rings of the tc isomers of $OsCl_2(tap)_2$ and $RuCl_2(pap)_2$[14] as in Figure 2. While the N–N distance follows the order Os > Ru, the C–N distances vary only slightly. It is concluded that the M–L π interaction increases as Ru < Os and that the interaction is primarily localized in the M–azo fragment. The systematic shortness of the M–N(azo) distance compared to the M–N(imine) distance in ruthenium[14] and osmium complexes of L (Figure 2) is a further indication of the presence of stronger M–azo π bonding. Clearly, the LUMO of L has a large azo character.

B. Reactivity of *trans,cis*-$OsX_2(tap)_2$. The bromo complex while being isomorphous with the chloro complex is the more reactive of the two. Therefore, it was chosen for all synthetic work. Even then, the reactivity is much less than that of the corresponding ruthenium complex. Thus, Ag^+-assisted halide displacement, which is facile in the case of ruthenium,[9] occurs

(15) Datta, D.; Chakravorty, A. *Inorg. Chem.* **1983**, *22*, 1085.
(16) The reaction solution (after removal of AgBr) is red-violet in color and displays multiple absorption bands (peaks at 840 and 492 nm with shoulders at 700 and 548 nm) in the visible region as expected of the $Os(tap)_2^{2+}$ moiety[13] (see also text). As in the case of[9] $Ru(H_2O)_2L_2^{2+}$, the bands are blue shifted (812, 640, 520, 492 nm) on addition of acetonitrile to the solution possibly due to displacement of H_2O by MeCN in the coordination sphere.
(17) Buckingham, D. A.; Dwyer, F. P.; Goodwin, H. A.; Sargeson, A. M. *Aust. J. Chem.* **1964**, *17*, 325.
(18) The mechanism of the substitution reaction is unknown at present. The long reaction times and the relatively severe reaction conditions would make meaningful kinetic characterization of the reactions extremely difficult. It is however known[7] that the halide substitution in RuX_2L_2 by tertiary phosphines proceeds by an associative mechanism attended with stereochemical rearrangement. A similar situation may be applicable to the reaction of *trans,cis*-$OsBr_2(tap)_2$ with bpy and phen.
(19) Chakravorty, A.; Kalia, K. C. *Inorg. Chem.* **1967**, *6*, 690.
(20) Mostad, A.; Rømming, C. *Acta Chem. Scand.* **1971**, *25*, 3561.
(21) Chang, C. H.; Porter, R. F.; Brauer, S. H. *J. Am. Chem. Soc.* **1970**, *92*, 5313.
(22) Roy, T.; Sengupta, S. P. *Cryst. Struct. Commun.* **1980**, *9*, 965.
(23) Fochi, G.; Floriani, C.; Bart, J. C. J.; Giunchi, G. *J. Chem. Soc., Dalton Trans.* **1983**, 1515.

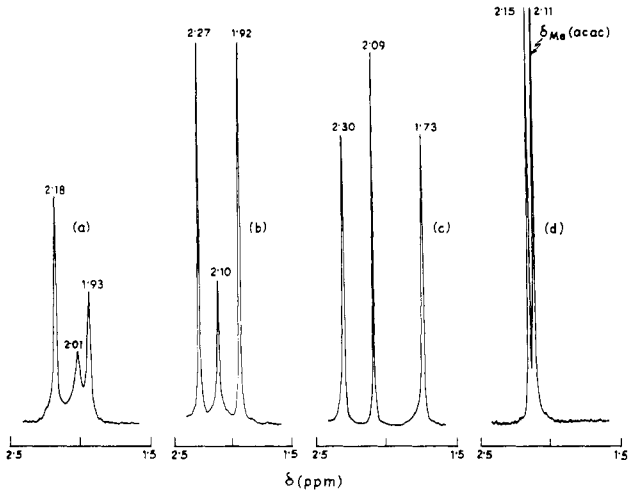

Figure 3. ^1H NMR methyl signals: (a) $[Os(tap)_3](ClO_4)_2 \cdot H_2O$; (b) $[Os(bpy)(tap)_2](ClO_4)_2 \cdot H_2O$; (c) $[Os(phen)(tap)_2](ClO_4)_2 \cdot H_2O$; (d) $[Os(acac)(tap)_2]Br$. The solvent is $(CD_3)_2SO$ except for (d) where it is $CDCl_3$.

only slowly and then when at least a 10-fold excess of silver ions are added to *trans,cis*-$OsBr_2(tap)_2$ in hot acidic aqueous methanol. Presumably reaction 2 occurs,[16] but we have not yet succeeded in isolating the diaquo complex in the pure state.

$$OsBr_2(tap)_2 + 2Ag^+ \rightarrow Os(H_2O)_2(tap)_2^{2+} + 2AgBr \quad (2)$$

The reaction of *trans,cis*-$OsBr_2(tap)_2$ with monobasic acids such as 2,4-pentanedione (Hacac), dibenzoylmethane (Hdbm), tropolone (Htrp), and glycine (Hgly) proceeds slowly but smoothly in boiling aqueous ethanol in the presence of suspended calcium carbonate, which neutralizes[17] the liberated acid. To hasten the reaction, the ligand is used in 10-fold excess. The red-violet complex cation $OsD(tap)_2^+$ is isolated in good yield as the perchlorate salt. The neutral oxalato complex $Os(ox)(tap)_2$ is afforded by reaction with sodium oxalate.

In the case of neutral N,N ligands (pap, tap, bpy, 1,10-phenanthroline (phen)), more drastic reaction conditions (prolonged boiling in aqueous 2-methoxyethanol) are required and even then the yields are poor. The orange-red cation $OsD(tap)_2^{2+}$ is again isolated as the perchlorate salt.

Elemental composition, solution electrical conductivity, and selected infrared frequencies of the new complexes are in Table II. The low values of $\nu_{N=N}$ are in full consonance with the Os–N(azo) π-bonding scheme considered in the previous section. The N=N frequencies in osmium complexes are systematically lower (by 20–40 cm^{-1}) than those in the ruthenium analogues.[14] This parallels the relative levels of $t_2 \rightarrow \pi^*$ donation; viz. Os > Ru as established from bond distance data (Figure 2).

C. ^1H NMR Spectra and Stereochemistry. The ^1H NMR spectra of selected complexes were examined to determine isomer composition. The tap methyl signal has been particularly useful in this respect. Thus, $Os(acac)(tap)_2^+$ displays separate and single Me(tap) and Me(acac) signals, suggesting that the C_2 symmetry[24] of the parent complex is retained. On the other hand, three such signals are present in the case of both $Os(bpy)(tap)_2^{2+}$ and $Os(phen)(tap)_2^{2+}$. Two of the three signals have equal heights (Figure 3). In these complexes the $Os(tap)_2^{2+}$ moiety is evidently present in both tc (one signal) and cc (two equal signals) geometries. Since the cc species is the major (Figure 3) constituent, extensive stereochemical rearrangement is occurring on substitution in these cases.[18]

(24) Even though the halves of molecule are slightly different in the crystal, in solution they are essentially identical as revealed by ^1H NMR data.[13]

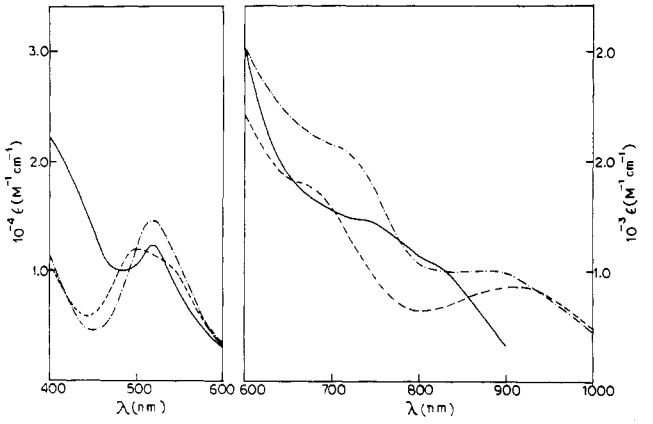

Figure 4. Electronic spectra of (a) $[Os(tap)_3](ClO_4)_2 \cdot H_2O$ (—), (b) $[Os(acac)(tap)_2]ClO_4 \cdot H_2O$ (–·–), and (c) $[Os(Gly)(tap)_2]ClO_4 \cdot H_2O$ (- - -) in acetonitrile.

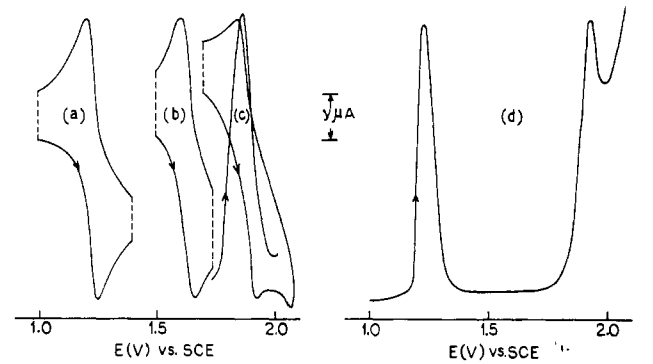

Figure 5. Voltammograms of (a) $[Os(bpy)_2(tap)](ClO_4)_2 \cdot H_2O$, (b) $[Os(bpy)(tap)_2](ClO_4)_2 \cdot H_2O$, (c) $[Os(tap)_3](ClO_4)_2 \cdot H_2O$, and (d) $[Os(acac)(tap)_2]ClO_4 \cdot H_2O$ in acetonitrile (0.1 M TEAP) at a platinum working electrode. For CV and DPV, $y = 10$ and 5, respectively. Scan rates and modulation amplitudes are as in Table IV.

The spectrum of $Os(tap)_3^{2+}$ is compatible[10,19] with a mixture of meridional and facial isomers of which the former is sterically favorable and is the major constituent. Isomer separation by chromatography has not been achieved.

It is significant that one of the methyl signals in the cc isomer of $Os(phen)(tap)_2^{2+}$ is significantly more shielded (δ_{Me} 1.73) than the corresponding signal in $Os(bpy)(tap)_2^{2+}$. In this isomer the two coordinating atoms of D and one azo nitrogen span an octahedral face. Examination of models shows that the *m*-tolyl ring attached to this azo nitrogen alone lies over[25] the phen (or bpy) ring. The stronger ring current in phen is believed to produce the observed effect.

D. Electronic Spectra. The complexes display multiple bands and shoulders in the region 220–1000 nm in acetonitrile solution (Table III; Figure 4). The absorptions occurring above[26] 450 nm are assigned to $t_2 \rightarrow \pi^*$ charge-transfer transitions where the π^* level has large azo character (vide supra). In d^6 metal ions, multiple $t_2 \rightarrow \pi^*$ charge-transfer transitions can arise[27-29] from low-symmetry splitting of the metal level, from the presence of more than one interacting

(25) This does not occur for the other *m*-tolyl ring of the cc isomer and for either of the two *m*-tolyl rings in the tc isomer.

(26) The intense transitions occurring below 450 nm are believed to be due to intraligand excitation and/or charge transfer involving antibonding ligand levels higher than the LUMO. The $n \rightarrow \pi^*$ and $\pi \rightarrow \pi^*$ transitions in free 2-(arylazo)pyridine are at[6] ~440 and ~320 nm.

(27) Pankuch, B. J.; Lacky, D. E.; Crosby, G. A. *J. Phys. Chem.* **1980**, *84*, 2061. Ceulemans, A.; Vanquickenborne, L. G. *J. Am. Chem. Soc.* **1981**, *103*, 2238.

(28) Decurtins, S.; Felix, F.; Ferguson, J.; Güdel, H. U.; Ludi, A. *J. Am. Chem. Soc.* **1980**, *102*, 4102.

(29) Kober, E. M.; Meyer, T. J. *Inorg. Chem.* **1982**, *21*, 3967.

Table II. Characterization Data

compd	molar conductivity[a] Λ, Ω^{-1} cm^2 M^{-1}	IR[b,c] ν_{max}, cm^{-1} C=N	IR[b,c] ν_{max}, cm^{-1} N=N	anal. data[d] % C	% H	% N
$[Os(tap)_3](ClO_4)_2 \cdot H_2O$	265	1598	1320	43.30 (43.29)	3.47 (3.53)	12.68 (12.62)
$[Os(pap)(tap)_2](ClO_4)_2 \cdot H_2O$	275	1600	1320	43.11 (42.68)	3.27 (3.38)	12.85 (12.80)
$[Os(bpy)(tap)_2](ClO_4)_2 \cdot H_2O$	275	1600	1300	42.30 (42.63)	3.25 (3.37)	11.60 (11.70)
$[Os(phen)(tap)_2](ClO_4)_2 \cdot H_2O$	270	1598	1298	43.87 (44.04)	3.19 (3.28)	11.66 (11.41)
$[Os(acac)(tap)_2]Br$	140	1600	1285	44.83 (45.27)	3.74 (3.83)	10.92 (11.01)
$[Os(acac)(tap)_2]ClO_4 \cdot H_2O$	145	1600	1285	43.68 (43.47)	3.78 (3.90)	10.57 (10.49)
$[Os(Gly)(tap)_2]ClO_4 \cdot H_2O$	155	1600	1285	40.46 (40.23)	3.56 (3.64)	12.78 (12.63)
$[Os(dbm)(tap)_2]ClO_4 \cdot H_2O$	160	1600	1285	50.94 (50.62)	3.72 (3.81)	9.24 (9.08)
$[Os(trp)(tap)_2]ClO_4 \cdot H_2O$	170	1600	1285	45.48 (45.23)	3.63 (3.55)	10.34 (10.21)
$[Os(ox)(tap)_2]$	10	1600	1282	46.21 (46.42)	3.41 (3.30)	12.56 (12.49)
$[Os(bpy)_2(tap)](ClO_4)_2 \cdot H_2O$	280	1600	1280	42.21 (41.92)	3.11 (3.19)	10.62 (10.70)

[a] Solvent is CH_3CN. [b] All bands are sharp and strong. [c] In KBr disk (4000–400 cm^{-1}). [d] Calculated values are in parentheses.

ligands (each contributing one π^* orbital), and from mixing of singlet and triplet configurations in the excited state[30] ($(t_2)^5(\pi^*)^1$) via spin–orbit coupling.

The osmium complexes like their ruthenium analogues[10,31] show one or two intense ($\epsilon \sim 10^4$) bands in the region 520 ± 50 nm. Here, the excited state is believed to be primarily singlet in character. On the other hand, only the osmium complexes have a relatively weak ($\epsilon \sim 10^3$) absorption above 800 nm. This is assigned to one or more triplet transitions, whose intensities are derived from singlet–triplet mixing due to strong spin–orbit coupling in osmium.[29]

E. Electrochemistry. The metal oxidation and ligand reduction behaviors of the complexes were probed in acetonitrile solution with the help of cyclic voltammetry (CV) and differential-pulse voltammetry (DPV). The chelates are found to act as carriers[32] of complete or nearly complete electron-transfer series. Results are in Table IV and Figures 5 and 6. All potentials are referenced to the saturated calomel electrode (SCE).

In the potential range +1.0 to +2.0 V, at least one reversible to quasi-reversible (peak-to-peak separation in CV 60–90 mV at a scan rate (v) of 50 mV s^{-1}) one-electron[33] oxidative response is observed at a platinum electrode in virtually all cases[34] corresponding to the couple 3. The osmium(III)–

$$Os^{III}DL_2^{(3-z)+} + e^- \rightleftharpoons Os^{II}DL_2^{(2-z)+} \quad (3)$$

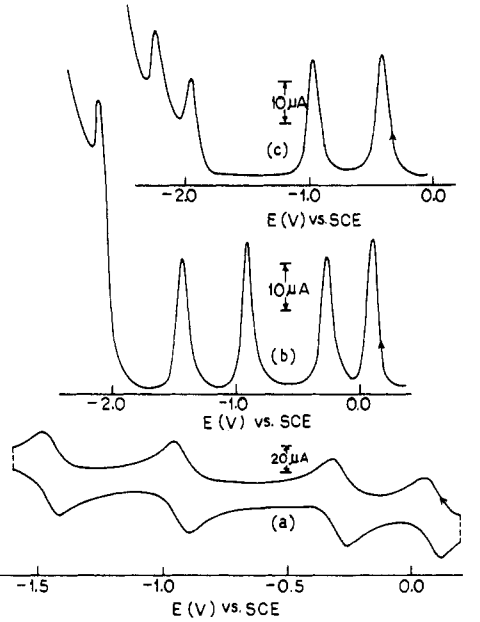

Figure 6. Voltammograms of (a) $[Os(pap)(tap)_2](ClO_4)_2 \cdot H_2O$, (b) $[Os(pap)(tap)_2](ClO_4)_2 \cdot H_2O$, and (c) $[Os(Gly)(tap)_2]ClO_4 \cdot H_2O$ in acetonitrile (0.1 M TEAP) at a glassy-carbon working electrode. Scan rates and modulation amplitudes are as in Table IV.

osmium(II) formal potential of $Os(bpy)_3^{2+}$ is[35] 0.81 V. On progressive replacement of bpy by L as in the series $Os(bpy)_3^{2+}$, $Os(bpy)_2(tap)^{2+}$, $Os(bpy)(tap)_2^{2+}$, and $Os(tap)_3^{2+}$, metal oxidation becomes more and more difficult. The formal potential (E°_{298} = 1.87 V) of $Os(tap)_3^{2+}$ represents the highest value so far reported[35-37] for osmium(III)–osmium(II) couples. The strong Os–azo π bonding is no doubt a contributing factor in making the E°_{298} values of couple 3 high. Quite generally, the osmium E°_{298} values are lower than the corresponding ruthenium[10] potentials, reflecting the relatively higher stability

(30) The ground state is a pure singlet as testified by sharp ^1H NMR spectra.
(31) The ruthenium complexes show a hitherto unreported shoulder on the lower enerlgy side of the ~520-nm band. In $Ru(tap)_3^{2+}$ and $Ru(acac)(tap)_2^+$ the shoulders are at 632 (ϵ 680) and 680 (ϵ 2240) nm, respectively.
(32) Vlček, A. A. *Coord. Chem. Rev.* **1982**, *21*, 785.
(33) The one-electron nature of each couple is established from comparison of current heights with those of standard one-electron systems.[10] Attempted coulometry at the required high potentials led to continuous counts.
(34) In the case of $Os(Gly)(tap)_2^+$ two overlapping anodic CV responses are seen at 1.24 and 1.34 V with little or no cathodic response on scan reversal (v = 50–100 mV s^{-1}). At high scan rates (>500 mV s^{-1}) the voltammogram becomes much better defined, with a single anodic response associated with a clearly defined cathodic counterpart—even though of unequal height. The anodic and cathodic peak potentials at v = 500 mV s^{-1} are 1.28 and 1.18 V, respectively. Evidently the complex undergoes a rate process on metal oxidation. The ligand reduction behavior of the complex is normal (see text).
(35) Kober, E. M.; Sullivan, B. P.; Dressick, W. J.; Caspar, J. V.; Meyer, T. J. *J. Am. Chem. Soc.* **1980**, *102*, 7383.
(36) Sullivan, B. P.; Meyer, T. J. *Inorg. Chem.* **1982**, *21*, 1037.
(37) Buckingham, D. A.; Dwyer, F. P.; Sargeson, A. M. *Inorg. Chem.* **1966**, *5*, 1243.

Table III. Electronic Spectral Data[a]

compd	λ_{max}, nm ($10^{-3}\epsilon$, M^{-1} cm^{-1})						
$[Os(tap)_3](ClO_4)_2 \cdot H_2O$	820[b] (1.05)	740[b] (1.45)	520 (12.11)	412[b] (20.83)	370 (25.40)	330 (25.80)	276 (19.45)	240[b] (10.51)	
$[Os(pap)(tap)_2](ClO_4)_2 \cdot H_2O$	820[b] (1.04)	744[b] (1.41)	664[b] (1.71)	520 (11.80)	412[b] (20.95)	370 (24.60)	330 (25.20)	274 (19.75)	240[b] (12.95)
$[Os(bpy)(tap)_2](ClO_4)_2 \cdot H_2O$	820[b] (0.86)	720[b] (1.01)	600[b] (1.65)	490 (12.48)	344 (20.84)	284 (26.12)	248[b] (8.86)		
$[Os(phen)(tap)_2](ClO_4)_2 \cdot H_2O$	820 (0.92)	724[b] (0.96)	600[b] (2.11)	492 (11.65)	340 (20.48)	286 (22.80)	248[b] (9.17)		
$[Os(acac)(tap)_2]ClO_4 \cdot H_2O$	890 (0.99)	720[b] (2.09)	616[b] (2.80)	518 (14.79)	346[b] (22.67)	318 (24.33)	260[b] (21.70)	230 (33.31)	
$[Os(Gly)(tap)_2]ClO_4 \cdot H_2O$	920 (0.83)	674[b] (1.76)	540[b] (10.32)	500 (11.93)	392[b] (11.60)	348[b] (18.91)	310 (21.92)	284[b] (20.20)	224 (28.36)
$[Os(dbm)(tap)_2]ClO_4 \cdot H_2O$	870 (0.97)	720[b] (1.91)	664[b] (2.38)	620[b] (2.88)	516 (13.25)	360[b] (26.71)	325 (44.38)	250[b] (27.95)	226 (34.11)
$[Os(trp)(tap)_2]ClO_4 \cdot H_2O$	950[b] (0.72)	740[b] (2.25)	640[b] (3.35)	520 (13.27)	340 (26.30)	296[b] (22.32)	234 (50.91)		
$[Os(ox)(tap)_2]$	900[b] (0.78)	780 (1.02)	680[b] (1.24)	566[b] (6.42)	508 (11.64)	346[b] (17.50)	318 (19.18)	226 (22.34)	
$[Os(bpy)_2(tap)](ClO_4)_2 \cdot H_2O$	820 (0.59)	612[b] (0.62)	476 (11.01)	440[b] (7.84)	376[b] (11.01)	304 (19.25)	256[b] (10.12)		

[a] Solvent is CH_3CN. [b] Shoulder.

Table IV. Electrochemical Data[a-d] at 298 K

compd	E°_{298}, V	
	metal-centered oxidn[e]	ligand-based redn[f]
$[Os(tap)_3](ClO_4)_2 \cdot H_2O$	1.87	0.11, −0.26, −0.91, −1.41, −2.07
$[Os(pap)(tap)_2](ClO_4)_2 \cdot H_2O$	1.86	0.10, −0.27, −0.91, −1.43, −2.09
$[Os(bpy)(tap)_2](ClO_4)_2 \cdot H_2O$	1.64	−0.22, −0.58, −1.45, −1.72, −2.38
$[Os(phen)(tap)_2](ClO_4)_2 \cdot H_2O$	1.62	−0.23, −0.60, −1.47, −1.72, −2.32
$[Os(acac)(tap)_2]ClO_4 \cdot H_2O$	1.23, 1.92	−0.40, −0.96, −1.95, −2.45
$[Os(Gly)(tap)_2]ClO_4 \cdot H_2O$	1.23[g]	−0.36, −0.94, −1.92, −2.19
$[Os(dbm)(tap)_2]ClO_4 \cdot H_2O$	1.26, 1.92	−0.39, −0.95, −1.82, −2.24
$[Os(trp)(tap)_2]ClO_4 \cdot H_2O$	1.12, 1.67	−0.39, −0.90, −1.89, −2.39
$[Os(ox)(tap)_2]$	1.15, 1.87	−0.43, −0.96, −2.01, −2.16
$[Os(bpy)_2(tap)](ClO_4)_2 \cdot H_2O$	1.23	−0.63, −1.17, −1.67, −2.07, −2.43

[a] Solvent CH_3CN; supporting electrolyte TEAP (0.1 M); solute concentration $\sim 10^{-3}$ M. [b] Unless otherwise stated both CV and DPV studies were made; the agreement between data obtained by the two techniques is invariably good (within ±5 mV). [c] In DPV the following parameters and relation were used: scan rate 10 mV s^{-1}; modulation amplitude (ΔE) is 25 mV; $E^\circ_{298} = E_p + 0.5(\Delta E)$, where E_p is the DPV peak potential. [d] In CV a scan rate of 50 mV s^{-1} was used unless otherwise stated; the relation $E^\circ_{298} = 0.5(E_{pc} + E_{pa})$ where E_{pc} and E_{pa} are cathodic and anodic peak potentials respectively was used to calculate the formal potential. [e] Working electrode is platinum. [f] Working electrode is glassy carbon. [g] Cyclic voltammetric data: scan rate 500 mV s^{-1}.

of the +3 oxidation state in the heavier metal. Even though several of the complexes exist as isomeric mixtures, only a single response for couple 3 is observed in each case, showing that the difference in the peak potentials of the isomers is unresolvably small. This is in line with the behavior of *trans,cis*-OsX_2L_2 and *cis,cis*-OsX_2L_2, which have[13] formal potentials within the very narrow range 0.94–0.96 V.

In the complexes where D is an O,O ligand, couple 3 occurs near 1 V and an additional one-electron response is seen at higher potentials most probably due to couple 4. Observation of couples at high (and low, see below) potentials near solvent cutoff is best made with DPV.

$$Os^{IV}DL_2^{(4-z)+} + e^- \rightleftharpoons Os^{III}DL_2^{(3-z)+} \qquad (4)$$

In the potential range +0.2 to −2.5 V multiple reductive responses are observed in acetonitrile solution at a glassy-carbon electrode (Table IV). The LUMO of L can accommodate[10] up to two electrons. Since this orbital has large azo character, this can be represented by (5). Four and six

$$-N{=}N- \overset{+e^-}{\rightleftharpoons} [-N\dot{-}\dot{N}-]^- \overset{+e^-}{\rightleftharpoons} [-N{-}N-]^{2-} \qquad (5)$$

successive one-electron reductions are therefore expected in OsL_2^{2+} and OsL_3^{2+} species. Four reductions are indeed seen in DPV[38] of $Os(gly)(tap)_2^+$ (Figure 6). The $OsDL_2^+$ species with O,O donors also behaves similarly (Table IV). In OsL_3^{2+} four reversible peaks (peak-to-peak separation 60 mV in each case) are seen in CV. In DPV a fifth response is seen overlying the solvent cutoff (Figure 6). Because of this overlap it is unclear whether the last response involves one or two electrons.[39] The behavior of OsL_3^{2+} is quite analogous to that[32,40]

(38) In CV only the first three responses are observable. The response at highest potential is obscured by solvent cutoff.

of $Os(bpy)_3^{2+}$ where bpy acts as a potential two-electron acceptor. The behavior of mixed bpy–L and phen–L complexes is in agreement with successive reduction of both types of ligands.

F. Concluding Remarks. Few structures of mononuclear osmium(II) complexes with unsaturated and conjugated nitrogenous ligands are reported in literature. The structure of *trans,cis*-$OsCl_2(tap)_2$ is therefore of special interest. The octahedral coordination sphere in this complex is not a surprise. The more important significance of the present work lies in clarifying the status of chelate rings **1** and **2** with regard to M → ligand π bonding. The Ru–N(imine) distance in Ru^{II}–bpy complexes[41] is virtually the same as that in $RuCl_2(pap)_2$.[10,14] Since π bonding in Ru^{II}–bpy is an accepted fact,[29] the shorter Ru–N(azo) distance (Figure 2) underlies the dominance of Ru^{II}–N(azo) π bonding. Whereas similar comparisons cannot be made in the case of osmium due to lack of available structural data on Os^{II}–bpy species, the same pattern should apply here too. This belief is supported by the relative bond distances of osmium(II) and ruthenium(II) complexes (Figure 2). A second important finding is that M–N(azo) π bonding clearly discriminates between the two metals, favoring the heavier one, as seen in N–N distances. Such discrimination is not observable for M–N(imine) π bonding in terms of C–N distances (Figure 2).

The feasibility of using OsX_2L_2 for the synthesis of $OsDL_2^{(2-z)+}$ has been established. The reactions are however slow, and stereochemical rearrangements do occur particularly when D is a neutral N,N ligand. The tris chelates systematically display spin-forbidden MLCT transitions that are not observed in the ruthenium analogues. These chelates along with their ruthenium counterparts[10] now constitute a well-characterized group where complete or nearly complete electron-transfer series are routinely observed—the metal undergoing one or two one-electron oxidations and each azoimine or α-diimine ligand taking in two electrons usually in different one-electron steps.

Experimental Section

Materials. The complexes *trans,cis*-$OsBr_2(tap)_2$[13] and $OsBr_2(bpy)_2\cdot H_2O$[17] were prepared as reported earlier. Dinitrogen was purified by bubbling it through an alkaline dithionite solution. The purification of acetonitrile and preparation of tetraethylammonium perchlorate (TEAP) for electrochemical work were done as before.[6] All other chemicals and solvents used for preparative works were reagent grade and were used without further purification.

Measurements. Electronic spectra were recorded with the use of either a Pye Unicam SP8-150 or Hitachi Model 330 spectrophotometer. Infrared spectra (KBr disk, 4000–400 cm^{-1}) were obtained with a Perkin-Elmer 783 spectrophotometer. ^1H NMR spectra were collected in $CDCl_3$ and $(CD_3)_2SO$ solvents on a Brucker 270-MHz spectrometer. Solution electrical conductivity was measured in a Philips PR9500 bridge with a solute concentration of $\sim 10^{-3}$ M. Electrochemical measurements were done with the help of a PAR Model 370-4 electrochemistry system: 174A polarographic analyzer; 175 universal programmer; RE0074 X-Y recorder. All experiments were carried out under dinitrogen atmosphere in a three-electrode configuration. A planar Beckman Model 39273 platinum electrode and PAR G0021 glassy-carbon electrodes were used as working electrodes. The results were collected at 298 ± 1 K and are referenced to a saturated calomel electrode (SCE). The reported potentials are uncorrected for junction contribution.

Preparation of Complexes. Tris[2-(*m*-tolylazo)pyridine]osmium(II) Perchlorate Monohydrate, $[Os(tap)_3](ClO_4)_2\cdot H_2O$. To a solution of 100 mg (0.134 mmol) of *trans,cis*-$OsBr_2(tap)_2$ in 30 mL of 2-methoxyethanol–water (2:1) was added 263 mg (1.34 mmol) of 2-(*m*-tolylazo)pyridine. The mixture was then heated to reflux for 40 h. The blue-violet solution gradually changed to orange-red. The solution was then evaporated on a water bath. The mass was dried in vacuo over P_4O_{10} and washed several times with benzene to remove excess ligand. The dried mass was dissolved in 10 mL of ethanol–water (2:1) saturated with sodium perchlorate. The solution was evaporated slowly in air. The precipitate was collected by filtration and washed thoroughly with cold water and finally with benzene. It was dried in vacuo over P_4O_{10} and subjected to chromatography on an alumina (S. Merck) column (20 × 1 cm). A small blue-violet band was eluted out with dichloromethane. A slower moving orange-red band was eluted out with benzene–acetonitrile (1:1). On slow evaporation of the eluant, the required complex was obtained in crystalline form; yield 25%.

The complex $[Os(pap)(tap)_2](ClO_4)_2\cdot H_2O$ (yield 26%) was prepared similarly. The complexes $[Os(bpy)(tap)_2](ClO_4)_2\cdot H_2O$ (yield 56%) and $[Os(phen)(tap)_2](ClO_4)_2\cdot H_2O$ (yield 55%) were also prepared by using the same solvent, procedure, and stoichiometry. The reaction time was however shorter (30 h).

(Acetylacetonato)bis[2-(*m*-tolylazo)pyridine]osmium(II) Bromide, $[Os(acac)(tap)_2]Br$. To a suspension of 100 mg (0.134 mmol) of *trans,cis*-$OsBr_2(tap)_2$ in 15 mL of ethanol–water (2:1) were added 134 mg (1.34 mmol) of acetylacetone and 135 mg (1.34 mmol) of calcium carbonate, and the mixture was heated to reflux for 8 h. The red-violet coloration gradually appeared with the progress of reaction. The solution was filtered, and the filtrate was evaporated slowly in air. The shining crystalline precipitate was collected by filtration and washed thoroughly with benzene. It was dried in vacuo over P_4O_{10}. The dried precipitate was redissolved in chloroform and filtered. The filtrate was evaporated slowly to dryness. The mass was then crystallized by slow evaporation from an ethanol–water (2:1) mixture; yield of dark crystals 75%.

The complex $[Os(acac)(tap)_2]ClO_4\cdot H_2O$ (yield 80%) was prepared by metathesis of $[Os(acac)(tap)_2]Br$ with sodium perchlorate in ethanol–water (2:1).

(Glycinato)bis[2-(*m*-tolylazo)pyridine]osmium(II) Perchlorate Monohydrate, $[Os(Gly)(tap)_2]ClO_4\cdot H_2O$. A 100-mg sample (1.34 mmol) of glycine and 135 mg (1.34 mmol) of calcium carbonate were added to a suspension of 100 mg (0.134 mmol) of *trans,cis*-$OsBr_2(tap)_2$ in 15 mL of ethanol–water (2:1) and heated to reflux for 8 h. During this period the suspension dissolved, producing a red-violet solution. This was filtered, and to the filtrate was added sodium perchlorate and this was evaporated slowly in air. The crystalline precipitate that deposited was collected by filtration and was washed with water and finally with benzene. Pure compound was obtained by column chromatography on neutral alumina (Glaxo Laboratories) with benzene–acetonitrile (1:1) as eluant; yield 70%.

The complexes $[Os(dbm)(tap)_2]ClO_4\cdot H_2O$ (yield 70%) and $[Os(trp)(tap)_2]ClO_4\cdot H_2O$ (yield 65%) were prepared from the same reaction stoichiometry and conditions.

(Oxalato)bis[2-(*m*-tolylazo)pyridine]osmium(II), $[Os(ox)(tap)_2]$. To a suspension of 100 mg (0.134 mmol) of *trans,cis*-$OsBr_2(tap)_2$ in 15 mL of ethanol–water (2:1) was added 180 mg (1.34 mmol) of sodium oxalate. The mixture was then heated to reflux for 8 h. The red-violet solution was concentrated and cooled. The precipitate thus formed was collected by filtration, washed thoroughly with water, and dried. It was then subjected to chromatography on a silica gel (BDH, 60–120 mesh) column (20 × 1 cm). A small blue-violet band was first eluted out with dichloromethane. Finally, the slow-moving red-violet bond was eluted out with benzene–acetonitrile (2:1). The required complex was obtained from the eluant in crystalline form by slow evaporation; yield 75%.

Bis(bipyridine)[2-(*m*-tolylazo)pyridine]osmium(II) Perchlorate Monohydrate, $[Os(bpy)_2(tap)](ClO_4)_2\cdot H_2O$. A 289-mg sample (1.47 mmol) of 2-(*m*-tolylazo)pyridine was added to a solution of 100 mg (0.147 mmol) of $OsBr_2(bpy)_2\cdot H_2O$ in 15 mL of ethanol–water (1:1). The mixture was then heated to reflux for 6 h, and the resulting solution was evaporated to dryness on a water bath and then dried further in vacuo over P_4O_{10}. The mass was washed with chloroform to remove excess ligand. The mass was dissolved in 10 mL of ethanol–water (2:1) saturated with sodium perchlorate. The solution was evaporated slowly in air. The resultant precipitate was collected by filtration and washed thoroughly with cold water and finally with chloroform. It was dried in vacuo over P_4O_{10}. The dried precipitate was recrystallized from dichloromethane–hexane (1:1), affording

(39) In RuL_3^{2+}, six responses are observed but the last two lie very close to each other. The observation of highly reduced species can be complicated by dissociation of reduced ligand as in the case[32,40] of $Os(bpy)_3^{2+}$.
(40) Roffia, S.; Raggi, M. A.; Ciano, M. *J. Electroanal. Chem. Interfacial Electrochem.* **1980**, *108*, 69.
(41) Rillema, D. P.; Jones, D. S.; Levy, H. A. *J. Chem. Soc., Chem. Commun.* **1979**, 849.

Table V. Selected Crystal Data, Data Collection Parameters, and Least-Squares Residuals

formula	$OsCl_2(C_{12}H_{11}N_3)_2$
fw	655.6
space group	$P2_1/c$
a, Å	8.035 (2)
b, Å	24.176 (4)
c, Å	13.416 (5)
β, deg	114.34 (3)
V, Å^3	2374
Z	4
d_{calcd}, g/cm^3	1.834
data collcn instrum	Enraf-Nonius CAD-4
radiation	graphite-monochromated Mo Kα (λ = 0.710 73 Å)
scan method	ω–2θ scan
cryst size, mm	0.27 × 0.15 × 0.075
μ(Mo Kα), cm^{-1}	59.41
range of θ, deg	$2 \leq \theta \leq 25$
no. of data, $I > 2\sigma(I)$	3326
no. of parameters refined	298
R[a]	0.026
R_w[b]	0.037
quality-of-fit indicator[c]	1.017
largest shift/esd	0.768

[a] $R = \Sigma||F_o| - |F_c||/\Sigma|F_o|$. [b] $R_w = [\Sigma w(|F_o| - |F_c|)^2/\Sigma w|F_o|^2]^{1/2}$, $w = \sigma^{-2}(F_o)$. [c] Quality-of-fit indicator = $[\Sigma w(|F_o| - |F_c|)^2/(N_{observns} - N_{parameters})]^{1/2}$.

crystals; yield 65%.

The IR spectra of all complexes were recorded in the range 4000–400 cm^{-1}. Selected frequencies are in Table II. All the perchlorate hydrates display characteristic ionic perchlorate bands at ~1080 cm^{-1} (broad and strong) and ~620 cm^{-1} (sharp and strong). In $[Os(acac)(tap)_2]ClO_4 \cdot H_2O$, $[Os(dbm)(tap)_2]ClO_4 \cdot H_2O$, and $[Os(trp)(tap)_2]ClO_4 \cdot H_2O$, characteristic β-diketone stretches occur at ~1530 and ~1515 cm^{-1}. In $[Os(ox)(tap)_2]$ carboxyl stretches are at 1710, 1680, and 1670 cm^{-1}. In $[Os(gly)(tap)_2]ClO_4 \cdot H_2O$, carboxyl and amine vibrations are seen at 1650 and 3300 cm^{-1}, respectively. Numerous other bands are observed in the complexes as expected.

Preparation of Crystals of *trans,cis*-$OsCl_2(tap)_2$ for X-ray Work. Hexane (5 mL) was layered over a solution of 2 mg of the complex in 5 mL of dichloromethane. Dark opaque crystals deposited in 10 days.

X-ray Structure Determination. A summary of crystal data, data collection parameters, and least-squares residuals are in Table V. The crystal used was black, opaque, and needle shaped. The unit cell dimensions and the orientation of the crystal with respect to the goniometer reference frame were given by a least-squares fit to the angular positions of 25 accurately located reflections. Systematic absences of the $0k0$ (k odd) and $h0l$ (l odd) reflections established the space group unambiguously.

The intensity values were corrected for Lorentz and polarization effects but not for absorption. The position of osmium atom was derived from the highest peaks of a Patterson map. The remaining 32 non-hydrogen atoms were located from successive Fourier maps and difference Fourier synthesis. One-cycle block-matrix least-squares refinement of the overall scale factor and positional and individual isotropic temperature factors of only the Cl, C, and N atoms resulted in an R factor of ~0.08. A weighting scheme based on empirical estimation of $\sigma(F)$[42] was adopted at this stage. Hydrogen atoms were detected and placed in calculated positions (C–H = 0.95 Å), and their contributions were included in structure factor calculations (B = 4.0 Å^2). The final refinement involved positional and anisotropic thermal parameters for all non-hydrogen atoms as well as an overall scale factor. Os was treated as an anomalous scatterer ($\Delta f'$ = −1.816, $\Delta f''$ = 7.605; ref 43). A difference Fourier map after convergence of the refinement showed no peaks of any chemical significance. Table VI gives the atomic coordinates and their estimated standard deviations for all non-hydrogen atoms.

Table VI. Positional and Isotropic Equivalent Thermal Parameters for *trans,cis*-$OsCl_2(tap)_2$[a,b]

atom	x	y	z	B_{eq}, Å^2
Os	0.12275 (4)	0.67907 (1)	0.26989 (2)	2.05
Cl(1)	0.2152 (3)	0.76379 (9)	0.2145 (2)	3.35
Cl(2)	−0.0615 (3)	0.73121 (9)	0.3379 (2)	3.32
N(1)	−0.1098 (8)	0.6690 (3)	0.1260 (5)	2.68
N(2)	0.3563 (8)	0.6844 (3)	0.4119 (5)	2.50
N(3)	0.0113 (8)	0.6105 (3)	0.2935 (5)	2.64
N(4)	0.3041 (8)	0.6364 (3)	0.2374 (5)	2.53
N(5)	0.4765 (9)	0.6331 (3)	0.3078 (6)	3.16
N(6)	−0.1490 (8)	0.5937 (3)	0.2246 (5)	3.06
C(1)	−0.167 (1)	0.6998 (3)	0.0343 (6)	2.85
C(2)	−0.333 (1)	0.6895 (4)	−0.0518 (6)	3.51
C(3)	−0.446 (1)	0.6485 (4)	−0.0437 (7)	3.56
C(4)	−0.389 (1)	0.6164 (4)	0.0495 (7)	3.36
C(5)	−0.219 (1)	0.6276 (3)	0.1337 (6)	2.76
C(6)	0.381 (1)	0.7092 (4)	0.5071 (6)	3.48
C(7)	0.551 (1)	0.7100 (4)	0.5948 (6)	3.78
C(8)	0.701 (1)	0.6871 (4)	0.5857 (6)	3.58
C(9)	0.679 (1)	0.6630 (4)	0.4873 (7)	3.44
C(10)	0.504 (1)	0.6611 (3)	0.4024 (6)	2.70
C(11)	0.263 (1)	0.6002 (3)	0.1450 (6)	2.87
C(12)	0.317 (1)	0.5449 (4)	0.1616 (7)	3.39
C(13)	0.273 (1)	0.5111 (4)	0.0704 (8)	4.21
C(14)	0.177 (1)	0.5324 (4)	−0.0342 (7)	4.18
C(15)	0.122 (1)	0.5873 (4)	−0.0500 (7)	3.38
C(16)	0.167 (1)	0.6215 (3)	0.0412 (6)	2.95
C(17)	0.167 (1)	0.5895 (4)	0.4886 (7)	3.56
C(18)	0.256 (1)	0.5515 (4)	0.5731 (7)	3.91
C(19)	0.275 (2)	0.4973 (4)	0.5457 (7)	4.91
C(20)	0.211 (2)	0.4806 (4)	0.4394 (9)	6.02
C(21)	0.122 (1)	0.5179 (4)	0.3545 (7)	3.99
C(22)	0.102 (1)	0.5713 (3)	0.3812 (7)	3.16
C(23)	0.010 (1)	0.6109 (4)	−0.1623 (7)	4.66
C(24)	0.331 (2)	0.5710 (6)	0.6905 (9)	6.72

[a] $B_{eq} = \frac{4}{3}[\beta_{11}a^2 + \beta_{22}b^2 + \beta_{33}c^2 + \beta_{13}ac\cos\beta]$. [b] Numbers in parentheses are estimated standard deviations in the least significant digits.

Crystallographic calculations were done on a Burroughs 6700 computer at the Regional Computer Centre, Calcutta. Programs used were from X-ray ARC package, extensively modified for local use. Weighted Fourier synthesis was done with NORMAL-EXFFT-SEARCH programs of the MULTAN 78 package.

Acknowledgment. Financial support received from the Department of Science and Technology, Government of India, New Delhi, is gratefully acknowledged. We are very thankful to Professor F. A. Cotton for providing the ORTEP diagram of *trans,cis*-$OsCl_2(tap)_2$.

Registry No. tc-$OsCl_2(tap)_2$, 93454-89-8; tc-$OsBr_2(tap)_2$, 93454-90-1; $[Os(tap)_3](ClO_4)_2$, 93454-92-3; $[Os(pap)(tap)_2](ClO_4)_2$, 93454-94-5; tc-$[Os(bpy)(tap)_2](ClO_4)_2$, 93454-96-7; cc-$[Os(bpy)(tap)_2](ClO_4)_2$, 93528-87-1; tc-$[Os(phen)(tap)_2](ClO_4)_2$, 93454-98-9; cc-$[Os(phen)(tap)_2](ClO_4)_2$, 93528-89-3; tc-$[Os(acac)(tap)_2]Br$, 93454-99-0; tc-$[Os(acac)(tap)_2]ClO_4$, 93455-01-7; $[Os(gly)(tap)_2]ClO_4$, 93455-03-9; $[Os(dbm)(tap)_2]ClO_4$, 93455-05-1; $[Os(trp)(tap)_2]ClO_4$, 93455-07-3; $[Os(ox)(tap)_2]$, 93455-08-4; $[Os(bpy)_2(tap)](ClO_4)_2$, 93455-10-8.

Supplementary Material Available: Listings of anisotropic thermal parameters (Table VII), parameters for hydrogen atoms (Table VIII), bond distances and bond angles (Table IX), least-squares planes and dihedral angles (Table X), and observed and calculated structure factors (26 pages). Ordering information is given on any current masthead page.

(42) Seal, A.; Ray, S. *Indian J. Phys.* **1981**, *55A*, 414.
(43) "International Tables of X-ray Crystallography"; Kynoch Press: Birmingham, England, 1974; Vol. 4.